Infection, Genetics and Evolution 67 (2019) 101–111

Contents lists available at ScienceDirect

Infection, Genetics and Evolution

journal homepage: www.elsevier.com/locate/meegid

Research paper

Molecular dynamics simulation analysis of conessine against multi drug resistant *Serratia marcescens*

Kalyani Dhusia[a], Kalpana Raja[b], Pierre Paul Michel Thomas[c], Pramod K. Yadav[a], Pramod W. Ramteke[d,*]

[a] Department of Computational Biology & Bioinformatics, Sam Higginbottom University of Agriculture, Technology and Sciences, Allahabad 211007, U.P., India
[b] Department of Dermatology, University of Michigan Medical School, Ann arbor, MI 48109, USA
[c] Institute of Public Health Genomics, Genetics and Cell Biology cluster, GROW Research School for Oncology and Developmental Biology, Maastricht University, the Netherlands
[d] Department of Biological Sciences, Sam Higginbottom University of Agriculture, Technology and Sciences, Allahabad 211007, U.P., India

ARTICLE INFO

Keywords:
Nosocomial diseases
Ornithine de carboxylase
Serratia
Molecular dynamics simulation

ABSTRACT

Ornithine decarboxylase (ODC) is an immediate precursor of polyamine biosynthesis in *Serratia marcescens* and a potential target for inhibition of its growth. We predicted the 3D structural conformation of ODC enzyme and validated it using MDS in our previous study. In this current study, the potential inhibitors of ODC were obtained by virtual screening of potential inhibitors from ZINC database and studied in depth for their different binding pose. Among the ten virtually screened inhibitors, Conessine exhibited the best binding with ODC and its inhibition property was studied further by MDS studies. The natural compound conessine is isolated from plant *Holarrhena antidysenterica* and it is studied against ODC of *Serratia marcenses* for its inhibitory potentials. This revealed unforeseen twisted position in root mean square fluctuation (RMSF) and ODC modelled conformation that influenced ligand binding. Both predicted model and ligand bound model were compared and found to be stable with Root Mean Square Deviation (RMSD) of approximately 7 nm and 0.25 nm to that of crystallographic structure over simulation time of 55 ns and 70 ns respectively. This work paves the way for future development of new drugs against nosocomial diseases caused by *Serratia marcescens*.

1. Introduction

Hospital-acquired or nosocomial outbreaks caused by *Serratia* spp. gram-negative bacilli of the *Enterobacteriaceae* have been reported in neonatal care units in both developing and developed countries (Bleckwenn et al., 2017; Morillo et al., 2016). Its ability to produce a beta lactamase, which facilitates resistance towards broad spectrum antibiotics has made treatment and management of these infections complicated (Kim et al., 2015; Moradigaravand et al., 2016; Phadke and Jacob, 2016).

Some infections may emerge from the patient's own body (skin otr intestinal microbiota) following an invasive procedure. The infection is then still considered nosocomial as it develops from the in a healthcare setting Almost 1.7 million hospital-associated infections resulting in 99,000 deaths each year in the United States alone is estimated by the Centers for Disease Control and Prevention (CDC) (Klevens et al., 2007). Outbreaks of hospital-acquired infections caused by methicillin-resistant *Staphylococcus aureus* are being reported with increasing frequency in the United States, but they are far behind the cases caused by Serratia. Also, research work has already been taken in reported against methicillin-resistant *Staphylococcus aureus*(Couvé-Deacon et al., 2017; Sampedro and Bubeck Wardenburg, 2017; Thompson et al., 1982).

Nosocomial infections accounts for two-thirds of the 25,000 deaths each year in Europe as per the hospital surveys states (Su et al., 2003). *S. marcescens* is now recognized as a prominent opportunistic pathogen causing significant outbreaks of nosocomial infections of various severities(Ostrowsky et al., 2002). Around 125,500 infected patients and almost 3000 deaths is caused due to nosocomial infection which constitutes about 6.2% of the total population in Belgium. Approximately €400 million/year of financial hike is observed in health insurances firms (Vrijens et al., 2009).

Antimicrobial resistance (AMR) is a growing threat to modern healthcare in both developed and developing countries (Sajjanar et al., 2017). Infections caused by bacteria carrying resistant genes are harder to treat and are correlated with higher mortality and morbidity

* Corresponding author.
E-mail address: pramod.ramteke@shiats.edu.in (P.W. Ramteke).

https://doi.org/10.1016/j.meegid.2018.11.001
Received 23 March 2018; Received in revised form 2 October 2018; Accepted 1 November 2018
Available online 02 November 2018

(Oliphant and Eroschenko, 2015). Infections with multi-drug resistance pathogens have also been associated with increased healthcare costs (Smith and Coast, 2013). These pathogens are particularly dangerous within hospitals where they cause nosocomial infections that present resistance to wide arrays of treatment regimens used inside the healthcare settings (Faidah et al., 2015). Infection with a drug-resistant, healthcare acquired infection (hereinafter HAIs) can prove fatal, especially for people with compromised immunity (Cabrera-Cancio, 2012). Lack of research in drugs against nosocomial infections in the last decades has led to a scarcity of molecules that remain effective against multidrug-resistant pathogens (Lee et al., 2013; Trubiano and Padiglione, 2015). Thus, there is a pressing need for novel treatment strategies to combat these resistant bacteria inside of healthcare settings.

From the 1960s onwards, *Serratia marcescens,* a gram-negative rod-shaped bacteria, was declared as ruthless human pathogen causing both opportunistic and healthcare-acquired infection (Yu, 1979). Only 2% of HAIs caused by *Serratia* spp. are identified and is constricted to clinical abrasions, the respiratory tract, the urinary tract and soft tissues. *Serratia* spp. causes meningitis and outbreaks often are reported in pediatrics wards (Mahlen, 2011).

Polyamines are synthesized from the amino acids either methionine, arginine (Fuhrmann et al., 2015; Gong et al., 2016) or ornithine by different life forms (Li et al., 2015; Miller-Fleming et al., 2015). The leading step in biosynthesis pathway of ornithine is the production of ornithine from glutamate by the mitochondrial enzyme acetylglutamate kinase (ArgEF) (Daidone et al., 2012; Mounce et al., 2016). Ornithine is then consequently decarboxylated by ODC (EC 4.1.1.17). Additionally, it should be noted that ornithine is essential for *Serratia* spp. survival as well. Thus, inhibition of ODC is a known approach for inhibition of ODC is a known pathway for growth inhibition (Dhusia et al., 2018b; Kurian et al., 2011; Mounce et al., 2016).

The Kyoto Encyclopedia for Genes and Genomes (KEGG) pathways deliberately provides that ornithine is the first intermediate step in the polyamine biosynthesis network of microorganisms (Haselbeck et al., 2013; Wallace and Fraser, 2004). The mechanism of *E. coli* for putrescine production using the ODC pathway was first reported by De Filippis and his coworkers in 2013 and the study indicates that ODC pathway is much more efficient for microbial production of putrescine and that ODC is a key enzyme in this pathway (De Filippis et al., 2013). Therefore, ODC with high catalytic efficiency will be advantageous for the economic production of putrescine by microorganisms. Here, we present structure-based virtual screening and dynamics simulation of ODC with its best inhibitor from natural products library from ZINC database.

2. Materials and methods

2.1. Identifying interacting proteins with ODC

The proteins interacting with ODC enzyme (EC 4.1.1.17) were obtained from the STRING database (Search Tool for the Retrieval of Interacting Genes/Proteins) (Djurhuus, 1981; Szklarczyk et al., 2015). The confidence value of retrieved interactions was set to 0.200 and the desired number of output interactions was set to 100. Cytoscape 3.3.0, (Su et al., 2014) a visualization tool was used to visualize protein interaction data. NCmine a module of Cytoscape was used to obtain the functional components of protein interactions. The nodes representing the same protein family were highlighted in same color (Tadaka and Kinoshita, 2016).

2.2. Molecular modeling and dynamics simulation

No NMR/crystal structure is available for ODC. However, a crystallographic Structure for a PLP-Dependent ODC from *Lactobacillus* (PDB id: 1ORD) (Momany et al., 1995), one mutant (PDB id: 1C4K) (Vitali et al., 1999) and four native X-ray crystallographic structures for arginine and lysine decarboxylase (PDB id: 2VYC, 4UPB, 5FKX and 3N75) from *E. coli* (Andréll et al., 2009; Kandiah et al., 2016; Kanjee et al., 2011; Malet et al., 2014; Sandmeier et al., 1994) are available in protein data bank (https://www.rcsb.org/pdb).

The intact sequence of ODC (NCBI- Protein accession number: AGE16259 and Uniprot id: L7ZQJ6_SERMA), was downloaded from UniProtKB/SwissProt (http://www.uniprot.org/uniprot/). Homology modeling was performed based on the crystallographic structure of ODC of *Lactobacillus* at 3.00 Å resolution (Protein Data Bank id: 1ORD) to obtain the model structure for ODC. The ODC enzyme shares a high sequence identity (56%) accompanied by 97% query coverage with chain A of crystallographic structure of ODC of *Lactobacillus* at 3.00 Å resolution. Tertiary structures of ODC were constructed using MODELLER version 9.15 (Webb and *Sali*, 2014). The PDB id 1ORD crystallographic structure was 730 amino acids long while that of ODC only constitutes 720 amino acids, with complete overlap. Hence, the predicted model was obtained without any truncation. Model selection from MODELLER generated structures was made on the basis of statistically potential models having comparable discrete optimized protein energy (DOPE) score (Shen and Sali, 2006).

2.2.1. Structural validation and energy minimization

The best 3D conformation was selected by considering *Z*-score from ProSA Web server, a protein structure analysis tool (Wiederstein and Sippl, 2007). ProSA calculates an overall quality with the Z-score of the submitted structures in pdb format. Based on similarity with Cα potentials or knowledge-based potentials of crystallographic and NMR structures that makes it suitable for even low-resolution structures.

MDS of 55 nanoseconds (ns) were performed on modelled ODC and compared with the crystallographic structure of *Lactobacillus* 1ORD in explicit solvent using Gromacs-5.1.4 program with Gromos96 all atom force field. Detailed discussion of parameters used are discussed in MDS section. Well defined averaged positioned 5 RMSF structures were obtained from simulation and visualized using PyMol available at http://www.pymol.org (Dhusia et al., 2016; Seeliger and De Groot, 2010). Model with least fluctuation was used further for active site prediction and screening studies.

Docking studies were performed using Autodock and Autogrid from the automated docking suite AutoDock 4. While AutoDock 4 performs the docking of inhibitors to a set of grids determining the target protein, Autogrid pre-calculates these grids (Morris et al., 2009; Park et al., 2006).

The choice of Autodock Vina as docking software was justified by its ability to identify bioactive conformations with a very good level of accuracy. Additionally, its high speed in docking is of great advantage while checking multiple inhibitors for same target.

The Autodock graphical interface AutoDockTools was used to keep polar hydrogens and add partial charges to the proteins using the Kollman United charges. The search space was included in a box of 48 × 36 × 56 Å, centered on the binding site of the ODC and conessine as ligand. Global and fexible docking has been done in this case using AutoDock vina.

2.3. Active site prediction and virtual screening

Structure-based virtual screening was used to explore the inhibitors for ODC. We used Indofine natural product library from ZINC database for identifying the potential inhibitors (Choi et al., 2014; Zhang et al., 2012). Our approach used docking and assigning scores to sort the candidate inhibitors in the virtual library. The docking predicts ligand conformation and orientation of the candidate inhibitors within the targeted active site. The scoring methods evaluate the binding interactions between the target and the candidate inhibitors. It is also useful to predict the biological activity of the natural compound based on the computed binding interactions. Autodock Vina (Trott and Olson, 2010;

Zhang et al., 2011) was used for virtual screening and it recognizes ligands and targets in pdbqt file format only. The potential inhibitors from ZINC database and ODC were converted to pdbqt file format using PERL script. ODC in pdbqt format is further optimized and minimized to obtain more stable configurations.

The active site in the modelled structure was predicted using the metaPocket 2.0 server (Zhang et al., 2011). This predicted multiple catalytic pockets with main residues (i.e. Gly200, Thr201, Ser202, Asp319, Ala321, Trp322, Lys357, Leu644 and Gln680) have been reported. Active site on the target molecule calculated earlier was cross validated from the literature of the template structure. Using the known coordinates, the Grid size and center were defined in prepared 3D structure of ODC.

2.4. Toxicity prediction using admetSAR

admetSAR is a free tool for evaluating chemical ADMET properties available at website (http://lmmd.ecust.edu.cn/admetsar1) (Cheng et al., 2012). Absorption, distribution, metabolism, excretion, and toxicity (ADMET) properties play vital roles in the discovery/development of drugs, natural products, and medically useful chemicals(Nisha et al., 2016; Ouassaf et al., 2018). This information is especially useful when to conduct human hazard assessment.

2.5. Molecular dynamics simulations

MDS of 55 ns for, modelled ODC of *Serratia* was performed using Gromacs-5.1.4 program with Gromos96 all atom force field (Hess et al., 2008) as already indicated in previous section for conformational sampling and secondary energy minimisation. The enzyme models were placed in a cubic box given distance 1.2 nm and solvated in a simple three-point water model (SPC) followed by the addition of Na + and Cl − to a concentration of 0.1 M. After steepest-descent energy minimization, 1-ns trajectories were calculated in a constant volume by 2 fs per step. The temperature was raised from 0 to 300 K in the first 50 ps and was maintained until the end. System was equilibrated under Normal Volume and Temperature (NVT) and Normal Pressure and Temperature (NPT) conditions for 100 ps respectively using the Parrinello-Rahman method to couple pressure isotropically to a value of 1.0 bar. During equilibrations, the protein backbone was restraint with a harmonic potential of force constant 1003 kJ/mol. The modified Berendsen (V-rescale) thermostat was employed to control the temperature of 300 K with a time constant of 50 ps. The first nanosecond of the simulation was considered to be an equilibration phase and was excluded from analysis. The enzymes ODC (EC 4.1.1.17) and ORD (EC 2.1.3.3) were simulated in a PLP free and substrate-free state (Fitjer et al., 1986).

MDS for 70 ns for ligand bound ODC (protein-ligand complex) of *Serratia* in explicit solvent using identical parameters as mentioned above was carried (Jee et al., 2017). In a search for dynamic behavior in active site residues that interacts with the substrate, we conducted separate simulations of Conessine bound to ODC as protein ligand complex. ODC was shown to find its niche between Leu644, Gln649, Ala650, Gln680 apparently forming hydrophobic and hydrogen bonds with the former.

2.6. Computing RMSF, RMSD and principal component analysis (PCA)

To understand and check the collective intramural kinesis of the enzymes and their complexes under consideration, PCA on the MD trajectories for up to 50 ns was carried out (Abdi and Williams, 2010; David and Jacobs, 2014). The B-factors of protein crystal structures reflect the fluctuation of atoms about their average positions and provide important information about protein dynamics (Soheilifard et al., 2008).

Amino acids in proteins which display highest B factors, pronounced maximum degree of thermal motion and hence more flexibility when considered into drug targeting. Hence the B-factor along with PCA was also calculated. Averaged B-factor structure is an unphysical structure but gives in-depth insight of the side chains and deciphered the effect of averaging over conformations.

For PCA, all the atoms in the protein were considered along with the residues from the terminals which express excessive random motion. An eigenvalue decomposition (EVD) of the covariance matrix leads to a complete set of orthogonal collective modes (eigenvectors), each with a corresponding eigenvalue (variance) that characterizes a portion of the motion, where larger eigenvalues describe motions on larger spatial scales. Overall translational and rotational motion were eliminated as they are irrelevant for the analysis of the internal motions of proteins. The covariance matrix was calculated using the option “covar” and the eigenvectors were analyzed using ‘anaeig’ in Gromacs (Cohen and Sternberg, 1980; Pitera, 2014).

The RMSF and RMSD were calculated from nanosecond-spaced polaroid shots superimposed onto the initial state using main-chain atoms. The inter-chain distances were tabulated for each residue for a series of Polaroid shots, and the distribution of the values was summarized by taking the quartiles (Fuglebakk et al., 2012).

3. Results

3.1. Network analysis of ODC

ODC protein-protein interaction network was obtained from STRING database and was analyzed in Cytoscape_v3.3.0. The initial dataset of ornithine interaction network deciphered interactions with the following KEGG pathways: Biosynthesis of amino acids [pathwayID 01230], arginine and proline metabolism [pathwayID 00330] and metabolic pathways [pathwayID 01100]. There were 144 interconnects thousands of edges, which were was sorted and restricted using Cytoscape. The interaction network data was then confined to antibiotics biosynthesis pathway containing 12 nodes and 32 edges as shown in Fig. 1. The STRING interactions are results of active prediction methods like neighbourhood, co-expression, experimental knowledge and text mining. Decarboxylase enzyme family included speB,

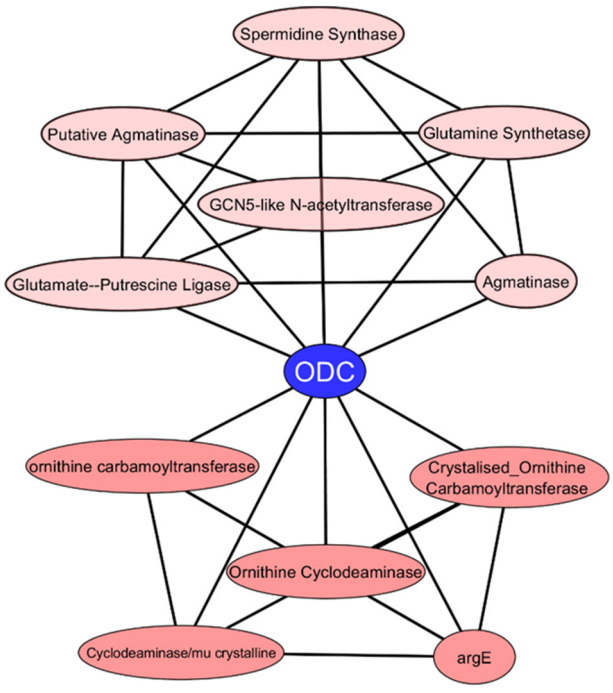

Fig. 1. Protein-protein interaction network of ODC.

Spro_1619, Spro_2068, speA, and Spro_4306 to be involved in curated pathway for superpathway of arginine, putrescine, and 4-aminobutyrate degradation. ODC was also found to play role in annotated pathway for pyrimidine metabolism. Pathway neighbors and subunits of the same enzyme/complex were given association links with thymidylate kinase (tmk), DNA polymerase III subunit delta' (Spro_1912), deoxycytidine triphosphate deaminase (dcd) and DNA polymerase III subunits gamma and tau (Spro_1135). ODC has a cliqueness value of 0.961, 0.780 and 0.307 with catalyzed formation of putrescine from agmatine, putrescine transporter family and arginine/ornithine antiporter family.

3.2. Structure modeling and validation

ODC protein was modelled using homology modeling technique and validated by MDS studies as described in our earlier report (Singh et al., 2016). The 3D model for ornithine decarboxylase enzyme chosen for further analysis was the top ranked predicted model using the chain A of the template protein ODC of *Lactobacilli* (PDB ID: 1ORD) using ProSA with *Z*-score of −10.87 (S2: Supplementary Fig. 1a) which makes it a closer fit for X-ray crystallographic structure. The plot of residue scores shows local model quality by plotting energies as a function of amino acid sequence position. A plot of single residue energies usually contains large fluctuations and is of limited value for model evaluation. Smoothed plot with average energy over each 40-residue fragment *s (i,i + 39)*, which is then assigned to the 'central' residue of the fragment at position *i + 19* is shown in S2: Supplementary Fig. 1b (thick green line). A second line with a smaller window size of 10 residues is shown in the background of the plot.

The sequences of both the proteins have 56% homology in amino acid sequence as obtained from the local alignment using modeller 9.15. The model validity was checked using Ramachandran plot assessment and 93% residues were found to fall under the allowed region.

To further remove the minor errors identified by ProSA (i.e, the region found in positive plot above the line in S2: Supplementary Fig1b) and PROCHECK server by analysis of the non-bonded interaction statistics using ERRAT showed that in ornithine enzyme has 2.4% residues (18/722) error in their folding.

To overcome these, a dynamics simulation was run for 50 ns and the averaged fluctuation structure was obtained by RMSF trajectory (Fig. 2) was then used for further virtual screening studies. The most fluctuating residues due to heavy residues positioned from 10 to 150 have been highlighted within inset with their 3D conformation against the superimposed crystallographic PDB model of 1ORD and RMSF model of predicted structure of ornithine decarboxylase of *Serratia* spp. Alpha carbon with backbone of both ODC and 1ORD were almost identical with a root mean square deviation of 0.4 Å. The RMSD study of the predicted model took 25 ns to stabilize itself in water medium. Since then the RMSD continued fluctuation in the range between 0.6 Å to 1.0 Å while crystallographic structure of 1ORD equilibrated itself in aqueous solvent after 10 ns and remained stable since then between 0.3 Å to 0.6 Å over the time index in ns.

3.3. Virtual screening

With the prepared executable files for virtual screening was performed on Autodock Vina from Indofine library of ZINC database. Out of which 10 ligands obtained after first screening (S2: Supplementary Fig. 2a), the best inhibitors on the basic of docking scores and inhibition profile were sorted out. The first virtual screening took Lipinski rule of five into its screening parameter against the target receptor site of ODC. For each natural compound the chemical structure is reported with their physical and chemical features in S2: Supplementary Fig. 2a and 2b. These ligands were namely; Conessine, Sumaresinolic acid (3–6-dihydroxy olean-12-en-28-oice acid), DNC (tetrandrine), Enoxolone, Naringenin, Hesperidin and Baicailin. Among the above noted natural inhibitors for polyamine biosynthesis, most of them had anomers (tautomers to be specific) hence a second run of screening was required for explicit results.

The second run for virtual screening took tautomarism of the screened molecules into account. Due to the change in single hydrogen (−H) bond orientation during the phenomenon called tautomarism the affinity energies rose from −9.7(Kcal/mol) to −9.5(Kcal/mol) then to −8.9 (Kcal/mol) in Conessine and from −9.2(Kcal/mol) to −8.8 (Kcal/mol) in Sumaresinolic acid. These gradual changes in binding affinity have been plotted in S2: Supplementary Fig. 2. Conessine had three enantiomers due to the orientation of hydrogen atoms at third and fourth positions. In first and second enantiomers of Conessine, H-4 was at front and back end of the plain of molecule and H-3 remained at back end. In third enantiomer both H-3 and H-4 atoms were placed at front

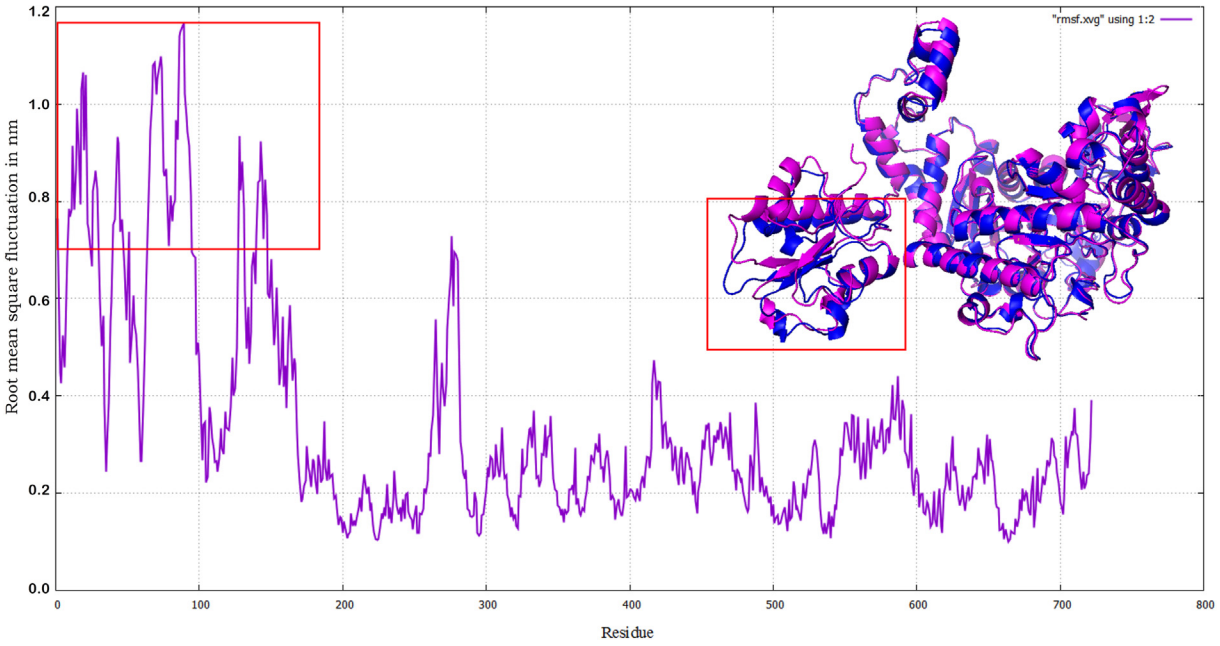

Fig. 2. RMSF of predicted model showing most fluctuating region and its corresponding change in orientation of structure within insets.

end.

Baicalin is a known prolyl endopeptidase inhibitor and is a flavone, type of flavonoid. It is found in several species in the genus *Scutellaria,* including *S. baicalensis* and *S. lateriflora*. Baicalin is the glucuronide of baicalein, and it is one of the chemical ingredients of Sho-Saiko-To which is an herbal supplement. DNC or tetrandra is obtained from herbaceous perennial vine of the Menispermaceae family native to China and Taiwan. It grows from a short, woodycaudex, climbing to a height of around three meters. The leaves are arranged spirally on the stem, and are peltate, i.e. with the leaf petiole attached near the center of the leaf.

In Autodock Vina the exhaustiveness option was set to 6, and all other options were kept at their default values. During the post-filtering phase, the poses of all inhibitors obtained in the previous structure-based virtual screening steps were ranked according to their score, obtained with the scoring function implemented in Autodock Vina. It should be noted that binding affinity data alone does not determine the overall potency of a drug. Potency is a result of the complex interplay of both the binding and ligand efficacy. Ligand efficacy refer to the ability of the ligand to produce to a biological response upon binding to the target receptor and the quantitative magnitude of this response. This response may be interpreted as an agonist or antagonist depending on the physiological response produced. The analysis of the inhibition profile against ODC of *S. marcescens* revealed that natural compounds are potential candidates as inhibitors of biosynthesis of antibiotics.

3.4. Binding analysis of ODC natural inhibitors

The natural compounds retrieved from the ZINC database after virtual screening were docked into the active site of ODC. The active site comprised of 12 residues as predicted by Meta pocket server and literature verification bound to the ligands with hydrophobic bonds.

The obtained complex was visually inspected to verify the absence of steric clashes between ligands and the residues at the active site. To this end, an energy grid with 48x36x56 (numbers refer to the number of grid points in xyz), centered on the e-amino group of the active site Gly293 of *Serratia marscens* was used.

During each docking simulation, grid dimension and center values were systematically maintained with other parameters. The selected values for grid dimension to the center of cavity were respectively $48 \times 36 \times 56$. However the coordinates $x = 81.242$ $y = 20.359$ $z = 31.887$ were also verified from literature and put to default for all the ligands. Water molecules were excluded from the docking calculations. All the docking and screening studies in this work were conducted using AutoDock. Three replicates were conducted for each ligand in the cross-docking and re-docking steps, while a dual cycle run was performed for screening.

All five sorted candidates after virtual screening were made to dock with target receptor using flexible docking. Their best docked possess with the enzyme have been captured using Pymol and shown in S2: Supplementary Fig. 3. Conessine was showing best docking score with least energy gives most stable complex. All three enantiomers of conessine are posed in ball and stick, dot view and default view respectively as shown in Fig. 3.

2D pictorial representation of the docked complexes using Ligplot^{+} tool delivers in depth insight of the positioning of potent inhibitors into the catalytic pockets of the enzyme. Hesperidin gets conjugated to the enzyme with the docking energy of −8.8 Kcal/mol, surrounded by residues Lys702, Pro 646, Val645, Arg653, Glu657 and Glu706 forming three hydrophobic bonds (shown in purple). There is no hydrogen bond formation hence this complex is discarded. Enoxolone ties to catalytic residues Pro646, Gly703, Try704, Ala656, Val703, Val643 and Phe637. Phe637 presents single hydrophobic bond with the target enzyme, stabilizing the complex to −8.9 kcal per joule. Baicalin bounds to the same cavity and same residue positions except for two extra residues namely Ile705 and Phe647.

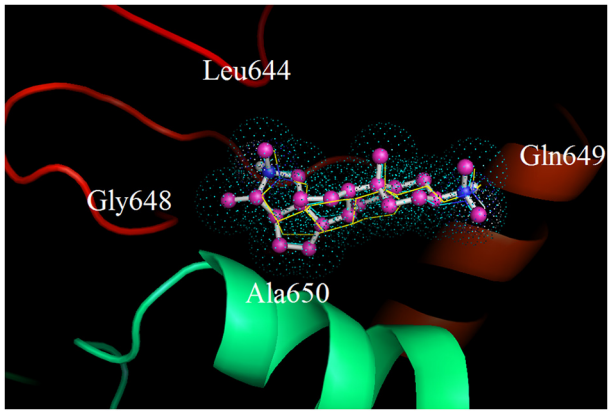

Fig. 3. Best docked orientation of conessine with ODC.

In spite of the fact that hersperidine, enoxolone and baicailine bind to the active site cavity, they were not taken into account because of the lack of hydrogen bonds formed with the active site residues. Hence these were not even considered for further analysis.

Hydrophobic interactions will not be able to outcast the stronger hydrogen bond formed by pyridoxal-5′-phosphate (PLP) dependent decarboxylases enzymes. Whereas conessine formed two hydrogen bonds with Gln680, Ala650 and Gln649 of bond length 2.90 Å, 3.33 Å and 3.06 Å respectively. These formed hydrogen bonds are clearly depicted in overlapped Ligplot view of PLP bound 1ORD against conessine ODC complex. Hydrogen and hydrophobic interactions are shown in green and red. Atoms of conessine are colored in black while that of 1ORD are in blue and red as referred in Fig. 4.

3.5. Toxicity prediction

The ADMET properties of Conessine as best inhibitor are discussed below in Table 1. The Caco-2 and HIA describes the intestinal absorption and as shown in table the value of Caco-2 Permeability for conessine is 0.6231 which is far below the toxicity level.

3.6. Dynamics simulation and analyzing principal components of 3D structures

To understand the comparative dynamic nature of ODC from *Serratia* spp. and *Lactobacilli*, we carried out MDS on the crystallographic structure and predicted model for 50 ns. ODC from *Serratia* spp. was found to be mechanically stable in comparison to that of 1ORD as seen from their RMSD, RMSF and gyration values over the simulation time. MD trajectory for conessine docked complex was comparatively dynamic proving its authenticated positioning into catalytic site of the ornithine precursor enzyme (Fig. 5, Movies of the molecular dynamics simulation are provided in: supplementary material S1).

3.6.1. Structural justification of ODC

PCA was conducted to generate the collective internal motions within the proteins under consideration on MD trajectories for up-to 50 ns. Like the crystallographic structure of 1ORD at 3 Å units, the residues from 1 to 106, consists of a three-stranded ß-sheet resembling to the seven stranded “wing” domain of 1ORD. Two wing domains of each dimer are present in 1ORD while ODC enzyme is a monomer with 3 ß-sheet and three helices present on the initial residues from residue number 49 to 55, 90 to 108 and 17 to 22 respectively. Other residues in this region show coiling with three sheets ranging from Ala37-Ser40, Tyr61-Val65 and Gly81-Ala84 projecting inwards stabilization. Leu109 to Asp191 links the outward initial residues to the main cluster chain with loops and coil entailing short helices separated by a loop. The third and major domain is organized with antiparallel loops forming deep

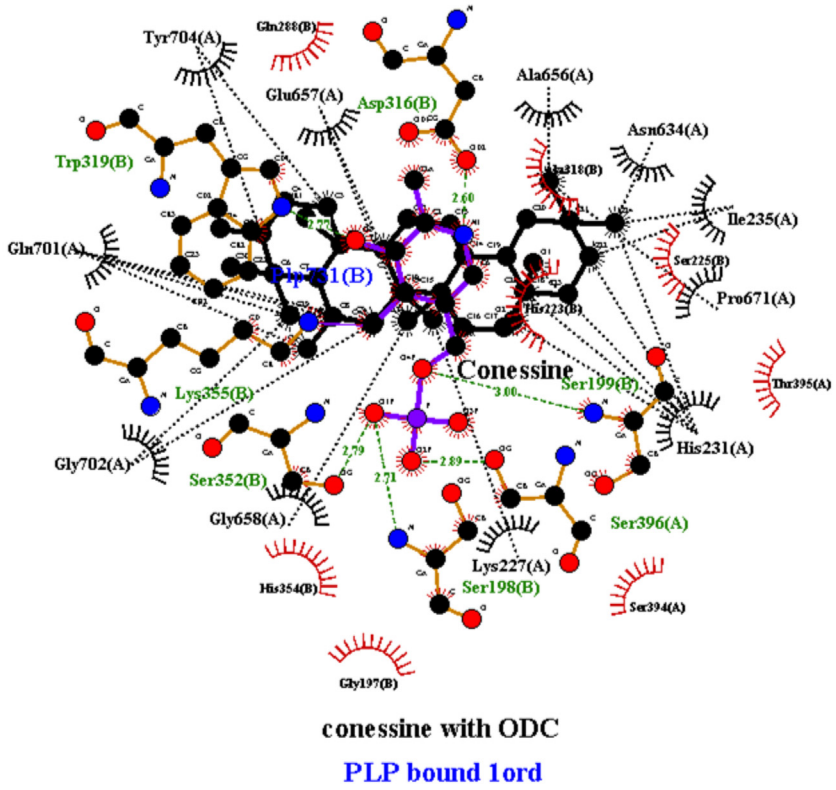

Fig. 4. Overlapped visualization of active site for docked modelled structure over PLP bound crystallographic structure.

Table 1
The tabulated ADME profile obtained from admetSAR server.

Absorption		Values are in %
Blood-brain barrier	BBB +	0.9767
Human intestinal absorption	HIA +	0.9970
Caco-2 permeability	Caco2 +	0.6231
P-glycoprotein substrate	Substrate	0.7635
P-glycoprotein inhibitor	Inhibitor	0.8834
	Inhibitor	0.9387
Renal organic cation transporter	Inhibitor	0.7095
Distribution		
Subcellular localization	Mitochondria	0.4159
Metabolism		
CYP450 2C9 substrate	Non-substrate	0.8288
CYP450 2D6 substrate	Non-substrate	0.6886
CYP450 3A4 substrate	Substrate	0.7718
CYP450 1A2 inhibitor	Non-inhibitor	0.9045
CYP450 2C9 inhibitor	Non-inhibitor	0.9071
CYP450 2D6 inhibitor	Non-inhibitor	0.9231
CYP450 2C19 inhibitor	Non-inhibitor	0.9025
CYP450 3A4 inhibitor	Non-inhibitor	0.8613
CYP Inhibitory promiscuity	Low CYP Inhibitory Promiscuity	0.6006
Excretion		
Toxicity		
Human ether-a-go-go-related gene inhibition	Weak inhibitor	0.8061
	Non-inhibitor	0.6185
AMES toxicity	Non AMES toxic	0.6048
Carcinogens	Non-carcinogens	0.9012
Fish toxicity	High FHMT	0.9837
Tetrahymena pyriformis toxicity	High TPT	0.8566
Honey bee toxicity	Low HBT	0.5407
Biodegradation	Not ready biodegradable	0.8894
Acute oral toxicity	III	0.6738
Carcinogenicity (Three-class)	Non-required	0.5984

channel for substrate binding with, residues 200 to 722, having thirteen stranded small and elongated ß-sheets and five stretched helices.

Both predicted model and ligand bound model were found to be stable with RMSD of approximately 7 nm and 0.25 nm to that of crystallographic structure over simulation trajectories as shown in S2: Supplementary Fig. 5a. Dynamics of active site of protein ligand complex has been studied and most stable pose is reported with its average RSMD, average RMSF, Radius of gyration and average potential energy as well as average SASA for the same in Table 2.

Above descriptions were proved by the statistical analysis of the solvent accessible surface area (SASA). It provides details of the surface area of the enzyme that is accessible for solvation commonly termed as solvent accessible surface (SAS). Its dynamics was calculated using the attributes gmx_sasa over time per residue and per atom. The averaged solvent accessible surface area of predicted model as well as ligand bound complex was higher as compared to that of crystallographic structure when indexed as per atom S2: Supplementary Fig. 4a. Similar pattern is depicted in case of averaged SASA over the residue index. 1ORD and ODC show maximum surface accessibility to 2 cubic nanometer area while that of complex hikes upto 2.17 nm^2 (see S2: Supplementary Fig. 4b).

Eigen value λp and eigenvector ν_q were obtained from construction and diagonalization of the covariance matrix of alpha-carbon randomness. The associated eigen value equals to the sum of the fluctuation described by the collective motion per atom, and thus is a measured for the total motility associated with an eigenvector. The comparative eigen value for the 10 units have been plotted for backbone chain of ODC and 1ORD, Protein-ligand complex and protein with side chain. Fig. 6a shows the above mentioned graphical plot and the same is validated by the box plot for the eigenvector in forth coming plot.

Eigenvalues were normalized to unit sum and the five largest eigen values were recorded as the first five. Accordingly, covariance matrices and their eigen values λp were calculated for 5 logarithmically spaced time windows ranging from 1 ns to 55 ns. For each window size,

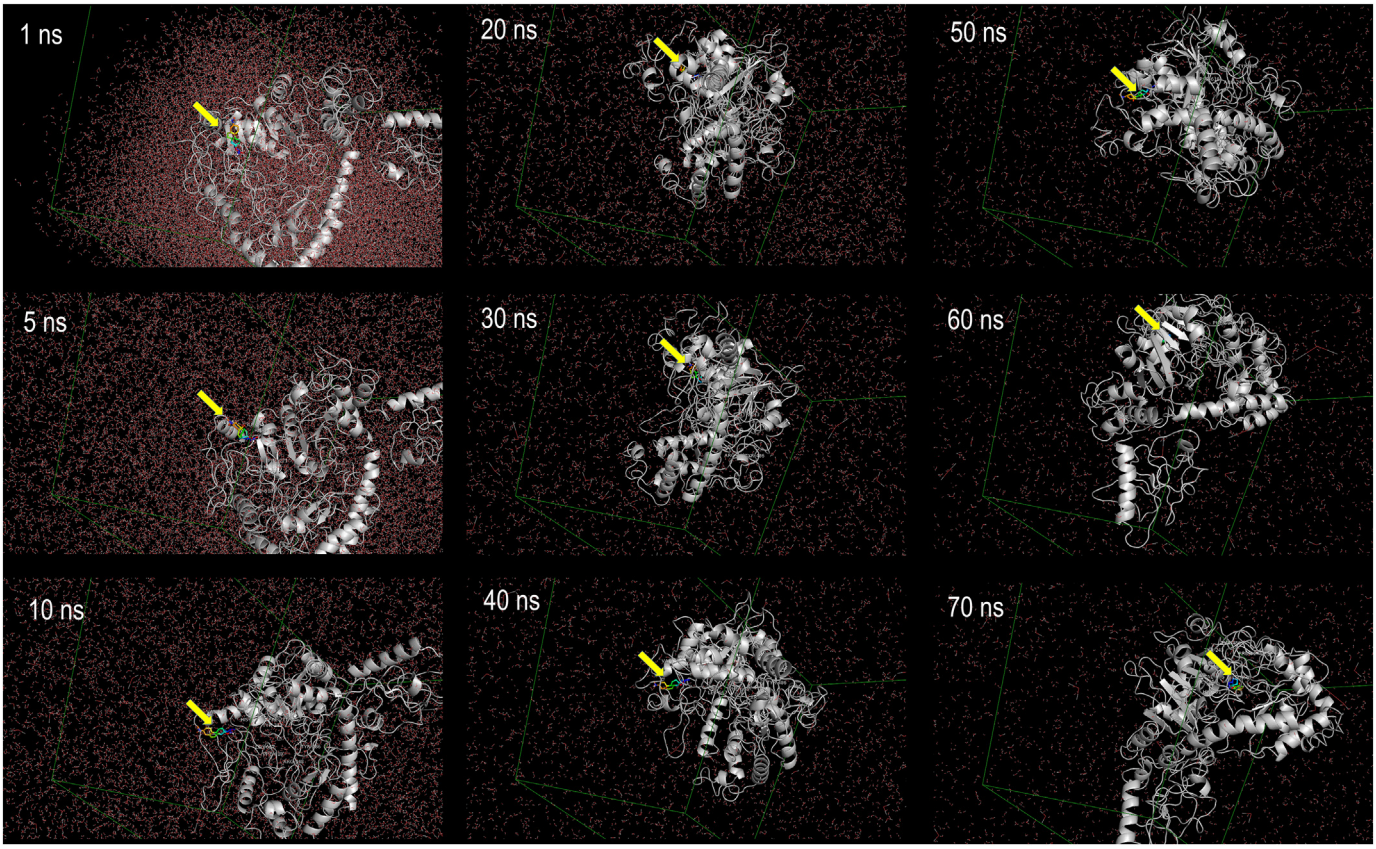

Fig. 5. Snapshots from the MDS of conessine bound ODC for 70 ns.

Table 2
The calculated parameters for all simulation systems obtained over complete trajectories.

Parameters	1ORD	ODC	Conessine bound ODC
Average potential energy (kJ/mol)	−1,709,176.81	−1,510,176.17	−1,411,487.72
Radius of gyration (nm)	2.95	2.77	2.84
Average RMSD (nm)	0.45	0.64	0.66
Average RMSF (nm)	0.5	0.7	2
Average SASA (nm^2)	309.95	295.75	283.55
B-factor (Å^2)	0.25	0.45	0.5
Density(kg/m^3)	1011.74	1012.19	998.78

eigenvalues were averaged over 5 uniformly distributed trajectory parts to reduce statistical fluctuations. The eigenvalues of the covariance matrix were calculated and arranged in order of decreasing value. The motion along the first five eigenvector directions is shown by projecting the trajectory onto these individual eigenvectors against time. Each of the eigenvectors describes a collective motion of particles, where the values of the vector indicate how much the corresponding atom participates in the motion. Since the eigenvalues are the average square displacements, the first eigenvectors represent the largest positional deviation, which is pictorially presented in Fig. 6a.

The projections of a trajectory on the eigenvectors of its covariance matrix are called principal components. It is often useful to check the cosine content of the principal component, since it is of random diffusion are cosines with the number of periods equal to half the principle component index. When a trajectory is projected on eigenvectors, all structures are fitted to the structure in the eigenvector file which in case of eigenvectors for structure under study are shown in Fig. 6b.

3.6.2. Dynamics insight of ligand bound state Vs. unliganded

To obtain insight into how inhibitor candidates affect the catalytic efficiency of the enzyme, molecular dynamics simulations was executed for enzyme in both ligand bound as well as unbound state and then compared to the MD trajectories of PLP-dependent crystallographic structure of ODC of *Lactobacillus*. The RMSF profiles revealed some interesting trends that can be correlated with their catalytic efficiency. The overall RMSF augmentedwith an increase in the catalytic efficiency as shown in S2: Supplementary Fig. 5b. Even though most of the dimer interfaces were highly rigid, α-helices and loops.

The most significant increase in RMSD was observed at the ligand entry site was observed in the docked ODC complex and the distance between pair residues was estimated to be 0.5 to 8.5 Å longer than unliganded structure (S2: Supplementary Fig. 5a). The MD trajectory of 70 ns for conessine bound ODC shows different conformations at same catalytic cavity. These posture indicate the adjustability of conessine in ODC and also helps in stabilizing the fluctuation in two hydrogen bonds formed. Different postures of ligand-protein complex are already shown for each 10 ns in Fig. 5. Although the overall pattern of the changes in RMSD was consistent among the simulations in these three sets, actual RMSD values differed between the experimental, modelled and the docked structures. The most consistent, minimum and maximum values of RMSD after 5 ns, till the end of the simulations for stable simulation runs are shown in Table 3.

On the other hand, RMSF had shown great fluctuation at the latter end of the plot after residue 720 as conessine was placed in input topology as HETATOM. Whereas the unliganded catalytic site had stable and continuous fluctuation and deviation as inferred from MD trajectories (S2: Supplementary Fig. 5c). The RMSF took a leap hike from 1.5 Å to 6 Å for conessine as inhibitor substrate. The radius of gyration (Rg) trajectories were calculated by simulation for 55 ns. Radius of gyration (Rg) is the measure of compactness of the structure providing the

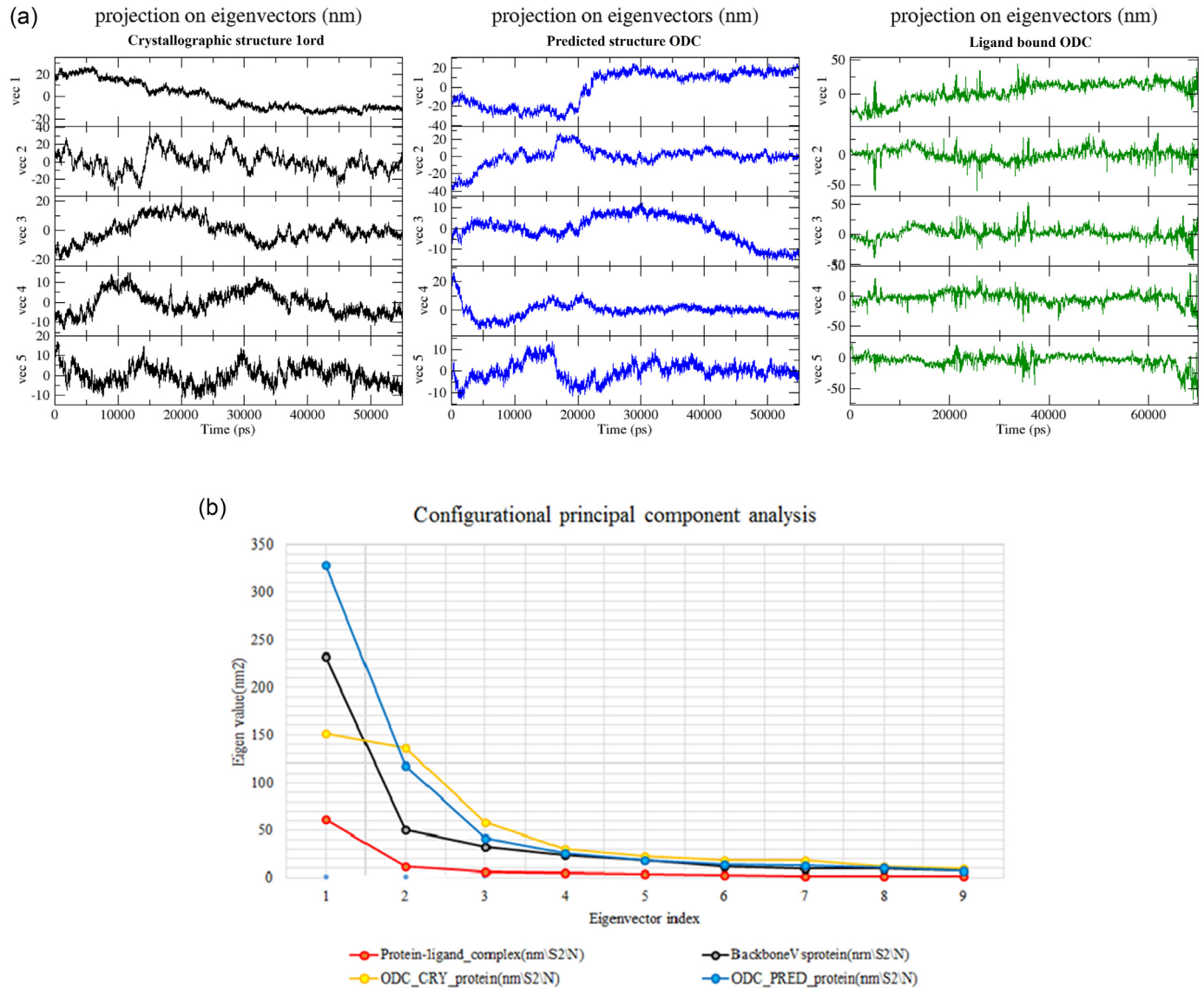

Fig. 6. a) The motions along the first five eigenvector directions for (i) Crystallographic structure 1ORD in black (ii) Predicted structure ODC in blue (iii) Ligand bound complex in green are shown by projecting the trajectory against time. b) Total positional fluctuations as a function of first 10 eigenvalues of crystallographic structure 1ORD (ii) Predicted structure ODC (iii) ligand bound complex and (iv) Backbone of ODC against eigenvector. (For interpretation of the references to color in this figure legend, the reader is referred to the web version of this article.)

Table 3
The RMSD values after 5 ns till the end for the stable simulation runs for each structure.

Structure	Simulation range (ns)	Consistent (nm)	Minimum (nm)	Maximum (nm)
1ORD	55	0.45	0.3	0.6
ODC	55	0.62	0.5	0.8
Conessine bound ODC	70	0.6	0.41	0.99

degree of the mass of the atom(s) relative to the center of mass of the molecule. S2: Supplementary Fig. 5d indicates the radius of gyration (Rg) for unbound state fluctuate at 2.85 Å while that for ligand bound state decreases to 2.75 Å indicating the compactness of enzyme when bound to conessine as substrate.

Another informative property with the MDS data is the number of hydrogen bonds formed (Protein – ligand H-bonding) between the ODC and the conessine. A Hydrogen bond is formed by attraction between the electron from hydrogen atom covalently bonded to an electronegative atom (donor) with another electronegative atom (acceptor).The presence or not of a hydrogen bond is inferred from the distance between a donor-H-acceptor pair and the donor-H-acceptor angle. In case of the protein structure the H-bonding with the intermolecules were calculated using the MD trajectories for 70 ns. The graphical plot for inter- molecular hydrogen bonding varies greatly in Fig. 7. The number of H-bonds for native structure of ODC raised up to 2 bonds due to interaction with conessine as ligand in water model.

Excessive fluctuation was observed when the ligand bound protein was solvated in water as medium and the H-bond were plotted in the same graph for comparative analysis. Water constitutes of two moles of hydrogen and one oxygen which provided major space for making and breaking of h-bond under solvation as depicted by dark green trajectory. These observations suggested the authenticity of the ligand binding at accurate site.

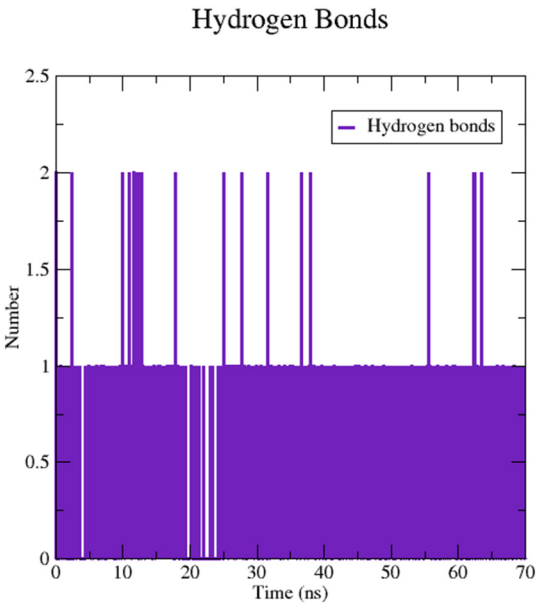

Fig. 7. Hydrogen bond fluctuation over the MD trajectory of 70 ns.

4. Discussion

In this paper, we investigated how much the correct ligand binding poses were maintained as stable poses were judged by the modern MDS. The possibility to distinguish the correct and incorrect docking poses only from the independent parallel MDS was also investigated. First, the high-quality data set of 7 complexes was created, which satisfied the typical physicochemical properties of the drug-like ligands. Above study along with case study by Roy and co-workers added evidence about the antimicrobial resistance of *Serratia* towards ampicillin, gentamycin, cefotaxime, ciprofloxacin, ceftazidime and even towards carbapenems (Khanna et al., 2013; Roy et al., 2014). There is hence a need for the development of novel strategies, other than antibacterial treatment to curb the growth of these pathogens that are naturally prone to the development of anti-microbial resistance. It should furthermore be stressed that additional measures, such as strict enforcement of infection control guidelines are necessary to ensure safe environments in healthcare settings (Gould, 2008). Prudent use of antimicrobials should also be advocated to prevent the development of multi-drug resistant pathogen (Gould, 2008). A safe ICU and hospital environment can only be achieved through concerted efforts at several levels of action (Zingg et al., 2015).

S. marcescens is a motile, short, rod-shaped, gram-negative, facultative anaerobic bacterium, classified in the large family *Enterobacteriaceae*. Along with other opportunistic and nosocomial pathogens, *S. marcescens* is involved in hospital-acquired infections, particularly catheter-associated bacteremia and urinary tract and wound infections (Khanna et al., 2013).

In November 2011, 7 isolates of *S. marcescens* were identified (six from the patients in the ICU and one from the soap dispenser in the ICU among a total of 327 isolates from the clinical samples of Sri Guru Ram Das Institute of Medical Sciences in India and 84 isolates were identified from the environmental sources in the ICU. This case study declared an outbreak of the *S. marcescens* due to the extrinsic contamination of the soap dispenser in the ICU. This also indicates the severity of the outbreak of disease caused by *Serratia* (Jenkins, 2017; Khanna et al., 2013).

In addition to the native pose from the crystal structure, the predicted and complex structures were generated by molecular modeling and docking software for each complex. Here, the high ranks of pose in top 10 candidate poses from docking score suggested that conessine is most stable ligand with predicted model and its MDS was performed.

Polyamines play important role in growth as well as stress and disease resistance by bacteria (Michael, 2016; Minocha et al., 2014; Minois et al., 2011).Furthermore, the agents are known to be regulators of cell growth and death. Hence it is likely that excess production of polyamines affects the severity and process of diseases (Minois et al., 2011; Mounce et al., 2016). Putrescine, spermidine and spermine are polyamines mainly found in microorganisms (Miller-Fleming et al., 2015; Saha et al., 2016). The leading step in biosynthesis pathway of polyamine is the production of ornithine from glutamate by the mitochondrial enzyme acetylglutamate kinase (ArgEF) (Daidone et al., 2012; Mounce et al., 2016). Ornithine is then consequently decarboxylated by ODC (ODC) to produce spermidine via putrescine (Gong et al., 2016) in the cytosol of *Serratia marscens strain WW4*. Hence for the controlled production of polyamines, conversion of ornithine into polyamine *vis* ODC should be stopped (Badieyan and Sobrado, 2013; Kurian et al., 2011). There is thus a need for development of specific ODC inhibitors with herbal ingredients to control polyamine accumulation (Badieyan and Sobrado, 2013).

Conessine was found to be the best inhibitor among the natural products from ZINC library. The steroidal alkaloid conessine isolated from the bark of *Holarrhena antidysentrica* (HA) is already known to exhibit substantial anti-malarial activity with slight cytotoxic nature in vitro.(Dua et al., 2013; Jamadagni et al., n.d.; Nondo et al., n.d.). HA is a medicinal plant abundantly found in India and is reported to be beneficial for the treatment of leukoderma and also for antihyperlipidemic activity(Jain, 2004; Sheikh et al., 2015).

It had three enantiomers due to the orientation of hydrogen atoms at third and fourth positions. In first and second enantiomers of conessine, H-4 was at front and back end of the plain of molecule and H-3 remained at back end. In third enantiomer both H-3 and H-4 atoms were placed at front end (Morais-Silva et al., 2016; Santora et al., 2008). In the face of chronic and emerging resistance of parasites to currently available drugs and constant need for new anti-malarials, natural plant products have been the bastion of anti-malarials for thousands of years. Moreover natural plant products and their derivatives have traditionally been a common source of drugs, and represent more than 30% of the current pharmaceutical market (Dua et al., 2013; Kim et al., 2016). Efforts should hence be geared towards advocacy and translational research in order to accelerate the development of active molecules that could be used in hospitals and healthcare settings.

5. Conclusions

Our work suggested that conessine (Zinc3977747) is currently the best inhibitor out of all screened potential inhibitors from Natural Library of ZINC database. The MD simulations have already provided the grounds for wet lab validations. Thus conessine is a potential inhibitor that can be used to overcome nosocomial disease virulence after successful to clinical trials. The isolated compound of conessine could be chemically modified to obtain a better potent chemical entity with no neuropsychiatric effects and improved characteristics as preclinical candidate against healthcare acquired infection(HAIs).

Supplementary data to this article can be found online at https://doi.org/10.1016/j.meegid.2018.11.001.

Equipment and settings

Sequence and structural alignments were carried out using NCBI blastp tool and Pymol. Structural figures and Columbian potential of surfaces were panelled using VMD and UCSF Chimera. Simulation graphs were prepared using Grace and Gnuplot.

Acknowledgements

We gratefully acknowledge the High Performance Computing (HPC)

Grid and Cloud Computing under Bioinformatics Resources & Applications Facility at C-DAC, Pune and Department of Computational Biology and Bioinformatics, SHUATS, Allahabad for providing computational infrastructure facility during this study.

Funding

This work was financially support by Rajiv Gandhi National Fellowship, University Grant Commission, India (RGNF-2015-17-SC-UTT-1664).

References

Abdi, H., Williams, L.J., 2010. Principal component analysis. Wiley Interdiscip. Rev. Comput. Stat. https://doi.org/10.1002/wics.101.

Andréll, J., Hicks, M.G., Palmer, T., Carpenter, E.P., Iwata, S., Maher, M.J., 2009. Crystal structure of the acid-induced arginine decarboxylase from Escherichia coli: reversible decamer assembly controls enzyme activity. Biochemistry 48, 3915–3927. https://doi.org/10.1021/bi900075d.

Badieyan, S., Sobrado, P., 2013. Hydroxylase: A Structure-Based Virtual Screening Study FAD. pp. 430–438.

Bleckwenn, M., Hammerschmidt, J., Rösing, C., Klaschik, M., 2017. Prevention of nosocomial infections and antibiotic resistance in nursing homes. Z. Gerontol. Geriatr. https://doi.org/10.1007/s00391-017-1262-y.

Cabrera-Cancio, M.R., 2012. Infections and the compromised immune status in the chronically critically Ill patient: prevention strategies. Respir. Care 57, 979–992. https://doi.org/10.4187/respcare.01621.

Cheng, F., Li, W., Zhou, Y., Shen, J., Wu, Z., Liu, G., Lee, P.W., Tang, Y., 2012. admetSAR: a comprehensive source and free tool for assessment of chemical ADMET properties. J. Chem. Inf. Model. 52, 3099–3105. https://doi.org/10.1021/ci300367a.

Choi, H., Kyeong, H.H., Choi, J.M., Kim, H.S., 2014. Rational design of ornithine decarboxylase with high catalytic activity for the production of putrescine. Appl. Microbiol. Biotechnol. 98, 7483–7490. https://doi.org/10.1007/s00253-014-5669-8.

Cohen, F.E., Sternberg, M.J.E., 1980. On the prediction of protein structure: the significance of the root-mean-square deviation. J. Mol. Biol. 138, 321–333. https://doi.org/10.1016/0022-2836(80)90289-2.

Couvé-Deacon, E., Mons, F., Garnier, F., Leduc, P., Ponthier, L., Domelier, M., Tristan, A., Ploy, M.-C., Pestourie, N., 2017. Neonatal outbreak of methicillin-resistant staphylococcus aureus clone geraldine: a bundle of measures to halt transmission. Infect. Control Hosp. Epidemiol. 38, 749–751. https://doi.org/10.1017/ice.2017.35.

Daidone, F., Montioli, R., Paiardini, A., Cellini, B., Macchiarulo, A., Giardina, G., Bossa, F., Borri Voltattorni, C., 2012. Identification by virtual screening and in vitro testing of human DOPA decarboxylase inhibitors. PLoS ONE 7. https://doi.org/10.1371/journal.pone.0031610.

David, C.C., Jacobs, D.J., 2014. Principal component analysis: a method for determining the essential dynamics of proteins. Methods Mol. Biol. 1084, 193–226. https://doi.org/10.1007/978-1-62703-658-0_11.

De Filippis, F., Pennacchia, C., Di Pasqua, R., Fiore, A., Fogliano, V., Villani, F., Ercolini, D., 2013. Decarboxylase gene expression and cadaverine and putrescine production by Serratia proteamaculans in vitro and in beef. Int. J. Food Microbiol. 165, 332–338. https://doi.org/10.1016/j.ijfoodmicro.2013.05.021.

Dhusia, K., Kesarwani, P., Yadav, P.K., 2016. Epitope prediction for MSP119 protein in Plasmodium yeolii using computational approaches. Netw. Model. Anal. Heal. Inform. Bioinforma. 5 (19). https://doi.org/10.1007/s13721-016-0127-4.

Dhusia, K., Yadav, P.K., Farmer, R., Ramteke, P.W., 2018b. Inhibition of polyamine biosynthesis for toxicity control in Serratia marcescens strain WW4 by targeting ornithine decarboxylase: a structure-based virtual screening study. Int. J. Comput. Biol. Drug Des. 11, 114–134. https://doi.org/10.1504/IJCBDD.2018.090837.

Djurhuus, R., 1981. Ornithine decarboxylase (EC 4.1.1.17) assay based upon the retention of putrescine by a strong cation-exchange paper. Anal. Biochem. 113, 352–355. https://doi.org/10.1016/0003-2697(81)90088-9.

Dua, V.K., Verma, G., Singh, B., Rajan, A., Bagai, U., Agarwal, D.D., Gupta, N., Kumar, S., Rastogi, A., 2013. Anti-malarial property of steroidal alkaloid conessine isolated from the bark of Holarrhena antidysenterica. Malar. J. 12. https://doi.org/10.1186/1475-2875-12-194.

Faidah, H.S., Ashgar, S.S., Barhameen, A.A.A., El-Said, H.M., 2015. Serratia Marcescens as Opportunistic Pathogen and the Importance of Continuous Monitoring of Nosocomial Infection in Makah City, Saudi Arabia. pp. 107–112. https://doi.org/10.4236/ojmm.2015.53013.

Fitjer, L., Majewski, M., Kanschik, A., Egert, E., Sheldrick, G.M., 1986. Synthesis and rearrangement of functionalized dispiro[2.1.3.3]Undecanes - preferred C4C5 over C3C4 ring enlargements. Tetrahedron Lett. 27, 3603–3606. https://doi.org/10.1016/S0040-4039(00)84860-1.

Fuglebakk, E., Echave, J., Reuter, N., 2012. Measuring and comparing structural fluctuation patterns in large protein datasets. Bioinformatics 28, 2431–2440. https://doi.org/10.1093/bioinformatics/bts445.

Fuhrmann, J., Clancy, K.W., Thompson, P.R., 2015. Chemical biology of protein arginine modifications in epigenetic regulation. Chem. Rev. 150513092954004. https://doi.org/10.1021/acs.chemrev.5b00003.

Gong, Z., Tang, M.M., Wu, X., Phillips, N., Galkowski, D., Jarvis, G.A., Fan, H., 2016. Arginine- and polyamine-induced lactic acid resistance in neisseria gonorrhoeae. PLoS ONE 11, e0147637. https://doi.org/10.1371/journal.pone.0147637.

Gould, I.M., 2008. Antibiotic policies to control hospital-acquired infection. J. Antimicrob. Chemother. 61, 763–765. https://doi.org/10.1093/jac/dkn039.

Haselbeck, R., Trawick, J.D., Niu, W., Burgard, A.P., 2013. Microorganisms for the Production of 1,4-Butanediol, 4-Hydroxybutanal, 4-Hydroxybutyryl-CoA, Putrescine and Related Compounds, and Methods Related Thereto.

Hess, B., Kutzner, C., van der Spoel, D., Lindahl, E., 2008. GROMACS 4: algorithms for highly efficient, load-balanced, and scalable molecular simulation. J. Chem. Theory Comput. 4, 435–447. https://doi.org/10.1021/ct700301q.

Jain, S.K., 2004. Credibility of traditional knowledge—the criterion of multilocational and multiethnic use. Indian J. Tradit. Knowl. 3, 137–153.

Jamadagni, P.S., Pawar, S.D., Jamadagni, S.B., Chougule, S., Gaidhani, S.N., Murthy, S.N., n.d. Review of *Holarrhena antidysenterica*(*L.*) Wall. ex A. DC.: pharmacognostic, pharmacological, and toxicological perspective. Pharmacogn. Rev. 11, 141–144. https://doi.org/10.4103/phrev.phrev_31_16

Jee, B., Kumar, S., Yadav, R., Singh, Y., Kumar, A., Sharma, N., 2017. Ursolic acid and carvacrol may be potential inhibitors of dormancy protein small heat shock protein16.3 of Mycobacterium tuberculosis. J. Biomol. Struct. Dyn. 1–10. https://doi.org/10.1080/07391102.2017.1389305.

Jenkins, D.R., 2017. Nosocomial infections and infection control. Medicine (Baltimore) 45, 629–633. https://doi.org/10.1016/j.mpmed.2017.07.005.

Kandiah, E., Carriel, D., Perard, J., Malet, H., Bacia, M., Liu, K., Chan, S.W.S., Houry, W.A., Ollagnier De Choudens, S., Elsen, S., Gutsche, I., 2016. Structural insights into the Escherichia coli lysine decarboxylases and molecular determinants of interaction with the AAA+ ATPase RavA. Sci. Rep. 6 (24601). https://doi.org/10.1038/srep24601.

Kanjee, U., Gutsche, I., Alexopoulos, E., Zhao, B., El Bakkouri, M., Thibault, G., Liu, K., Ramachandran, S., Snider, J., Pai, E.F., Houry, W.A., 2011. Linkage between the bacterial acid stress and stringent responses: the structure of the inducible lysine decarboxylase. EMBO J. 30, 931–944. https://doi.org/10.1038/emboj.2011.5.

Khanna, A., Khanna, M., Aggarwal, A., 2013. Serratia marcescens- a rare opportunistic nosocomial pathogen and measures to limit its spread in hospitalized patients. J. Clin. Diagn. Res. 7, 243–246. https://doi.org/10.7860/JCDR/2013/5010.2737.

Kim, S.B., Jeon, Y.D., Kim, J.H., Kim, J.K., Ann, H.W., Choi, H., Kim, M.H., Song, J.E., Ahn, J.Y., Jeong, S.J., Ku, N.S., Han, S.H., Choi, J.Y., Song, Y.G., Kim, J.M., 2015. Risk factors for mortality in patients with Serratia marcescens bacteremia. Yonsei Med. J. 56, 348–354. https://doi.org/10.3349/ymj.2015.56.2.348.

Kim, H., Lee, K. Il, Jang, M., Namkoong, S., Park, R., Ju, H., Choi, I., Oh, W.K., Park, J., 2016. Conessine interferes with oxidative stress-induced C2C12 myoblast cell death through inhibition of autophagic flux. PLoS ONE 11, e0157096. https://doi.org/10.1371/journal.pone.0157096.

Klevens, R.M., Edwards, J.R., Richards, C.L., Horan, T.C., Gaynes, R.P., Pollock, D.A., Cardo, D.M., 2007. Estimating health care-associated infections and deaths in U.S. hospitals, 2002. Public Health Rep. 122, 160–166. https://doi.org/10.1177/003335490712200205.

Kurian, L., Palanimurugan, R., Gödderz, D., Dohmen, R.J., 2011. Polyamine sensing by nascent ornithine decarboxylase antizyme stimulates decoding of its mRNA. Nature 477, 490–494. https://doi.org/10.1038/nature10393.

Lee, C.R., Cho, I.H., Jeong, B.C., Lee, S.H., 2013. Strategies to minimize antibiotic resistance. Int. J. Environ. Res. Public Health. https://doi.org/10.3390/ijerph10094274.

Li, K., Chen, W.H., Bruner, S.D., 2015. Structure and mechanism of the siderophore-interacting protein from the fuscachelin gene cluster of thermobifida fusca. Biochemistry 54, 3989–4000. https://doi.org/10.1021/acs.biochem.5b00354.

Mahlen, S.D., 2011. Serratia infections: from military experiments to current practice. Clin. Microbiol. Rev. https://doi.org/10.1128/CMR.00017-11.

Malet, H., Liu, K., El Bakkouri, M., Chan, S.W. ah S., Effantin, G., Bacia, M., Houry, W.A., Gutsche, I., 2014. Assembly principles of a unique cage formed by hexameric and decameric *E. coli* proteins. Elife e03653, 3. https://doi.org/10.7554/eLife.03653.

Michael, A.J., 2016. Polyamines in eukaryotes, bacteria, and archaea. J. Biol. Chem. 291, 14896–14903. https://doi.org/10.1074/jbc.R116.734780.

Miller-Fleming, L., Olin-Sandoval, V., Campbell, K., Ralser, M., 2015. Remaining mysteries of molecular biology: the role of polyamines in the cell. J. Mol. Biol. 427, 3389–3406. https://doi.org/10.1016/j.jmb.2015.06.020.

Minocha, R., Majumdar, R., Minocha, S.C., 2014. Polyamines and abiotic stress in plants: a complex relationship. Front. Plant Sci. 175 (11–17), 5. https://doi.org/10.3389/fpls.2014.00175.

Minois, N., Carmona-Gutierrez, D., Madeo, F., 2011. Polyamines in aging and disease. Aging (Albany NY) 3, 716–732. https://doi.org/10.1016/S0044-8486(03)00351-X.

Momany, C., Ernst, S., Ghosh, R., Chang, N.L., Hackert, M.L., 1995. Crystallographic structure of a PLP-dependent ornithine decarboxylase from Lactobacillus 30a to 3.0 a resolution. J. Mol. Biol. 252, 643–655. https://doi.org/10.1006/jmbi.1995.0526.

Moradigaravand, D., Boinett, C.J., Martin, V., Peacock, S.J., Parkhill, J., 2016. Recent independent emergence of multiple multidrug-resistant Serratia marcescens clones within the United Kingdom and Ireland. Genome Res. 26, 1101–1109. https://doi.org/10.1101/gr.205245.116.

Morais-Silva, G., Ferreira-Santos, M., Marin, M.T., 2016. Conessine, an H3 receptor antagonist, alters behavioral and neurochemical effects of ethanol in mice. Behav. Brain Res. 305, 100–107. https://doi.org/10.1016/j.bbr.2016.02.025.

Morillo, Á., González, V., Aguayo, J., Carreño, C., Torres, M.J., Jarana, D., Artacho, M.J., Jiménez, F., Conde, M., Aznar, J., 2016. A six-month Serratia marcescens outbreak in a neonatal intensive care unit. Enferm. Infecc. Microbiol. Clin. 34, 645–651. https://doi.org/10.1016/j.eimc.2016.01.006.

Morris, G.M., Huey, R., Lindstrom, W., Sanner, M.F., Belew, R.K., Goodsell, D.S., Olson, A.J., 2009. AutoDock4 and AutoDockTools4: automated docking with selective receptor flexibility. J. Comput. Chem. 30, 2785–2791. https://doi.org/10.1002/jcc.21256.

Mounce, B.C., Cesaro, T., Moratorio, G., Hooikaas, P.J., Yakovleva, A., Werneke, S.W., Smith, E.C., Poirier, E.Z., Simon-Loriere, E., Prot, M., Tamietti, C., Vitry, S., Volle, R., Khou, C., Frenkiel, M.-P., Sakuntabhai, A., Delpeyroux, F., Pardigon, N., Flamand, M., Barba-Spaeth, G., Lafon, M., Denison, M.R., Albert, M.L., Vignuzzi, M., 2016. Inhibition of polyamine biosynthesis is a broad-spectrum strategy against RNA viruses. J. Virol. JVI. https://doi.org/10.1128/JVI.01347-16. 01347–16.

Nisha, C.M., Kumar, A., Vimal, A., Bai, B.M., Pal, D., Kumar, A., 2016. Docking and ADMET prediction of few GSK-3 inhibitors divulges 6-bromoindirubin-3-oxime as a potential inhibitor. J. Mol. Graph. Model. 65, 100–107. https://doi.org/10.1016/j.jmgm.2016.03.001.

Nondo, R.S.O., Erasto, P., Moshi, M.J., Zacharia, A., Masimba, P.J., Kidukuli, A.W., n.d. In vivo antimalarial activity of extracts of Tanzanian medicinal plants used for the treatment of malaria. J. Adv. Pharm. Technol. Res. 7, 59–63. https://doi.org/10.4103/2231-4040.179748

Oliphant, C.M., Eroschenko, K., 2015. Antibiotic resistance, part 2: gram-negative pathogens. J. Nurs. Pract. 11, 79–86. https://doi.org/10.1016/j.nurpra.2014.10.008.

Ostrowsky, B.E., Whitener, C., Bredenberg, H.K., Carson, L.A., Holt, S., Hutwagner, L., Arduino, M.J., Jarvis, W.R., 2002. Serratia marcescens bacteremia traced to an infused narcotic. N. Engl. J. Med. 346, 1529–1537. https://doi.org/10.1056/NEJMoa012370.

Ouassaf, M., Belaidi, S., Lotfy, K., Daoud, I., Belaidi, H., 2018. Molecular docking studies and ADMET properties of new 1.2.3 triazole derivatives for anti-breast cancer activity. J. Bionanosci. 12, 26–36. https://doi.org/10.1166/jbns.2018.1505.

Park, H., Lee, J., Lee, S., 2006. Critical assessment of the automated AutoDock as a new docking tool for virtual screening. Proteins Struct. Funct. Genet. 65, 549–554. https://doi.org/10.1002/prot.21183.

Phadke, V.K., Jacob, J.T., 2016. Marvelous but morbid: infective endocarditis due to Serratia marcescens. Infect. Dis. Clin. Pract. 24, 143–150. https://doi.org/10.1097/IPC.0000000000000360.

Pitera, J.W., 2014. Expected distributions of root-mean-square positional deviations in proteins. J. Phys. Chem. B 118, 6526–6530. https://doi.org/10.1021/jp412776d.

Roy, P., Ahmed, N.H., Grover, R.K., 2014. Non-pigmented strain of Serratia marcescens: an unusual pathogen causing pulmonary infection in a patient with malignancy. J. Clin. Diagn. Res. 8, 5–6. https://doi.org/10.7860/JCDR/2014/8629.4513.

Saha, M., Sarkar, S., Sarkar, B., Sharma, B.K., Bhattacharjee, S., Tribedi, P., 2016. Microbial siderophores and their potential applications: a review. Environ. Sci. Pollut. Res. 23, 3984–3999. https://doi.org/10.1007/s11356-015-4294-0.

Sajjanar, B., Dhusia, K., Saxena, S., Joshi, V., Bisht, D., Thakuria, D., Manjunathareddy, G.B., Ramteke, P.W., Kumar, S., 2017. Nicotinic acetylcholine receptor alpha 1(nAChRα1) subunit peptides as potential antiviral agents against rabies virus. Int. J. Biol. Macromol. 104, 180–188. https://doi.org/10.1016/j.ijbiomac.2017.05.179.

Sampedro, G.R., Bubeck Wardenburg, J., 2017. Staphylococcus aureus in the intensive care unit: are these golden grapes ripe for a new approach? J. Infect. Dis. 215, S64–S70. https://doi.org/10.1093/infdis/jiw581.

Sandmeier, E., Hale, T.I., Christen, P., 1994. Multiple evolutionary origin of pyridoxal-5′-phosphate-dependent amino acid decarboxylases. Eur. J. Biochem. 221, 997–1002. https://doi.org/10.1111/j.1432-1033.1994.tb18816.x.

Santora, V.J., Covel, J.A., Hayashi, R., Hofilena, B.J., Ibarra, J.B., Pulley, M.D., Weinhouse, M.I., Sengupta, D., Duffield, J.J., Semple, G., Webb, R.R., Sage, C., Ren, A., Pereira, G., Knudsen, J., Edwards, J.E., Suarez, M., Frazer, J., Thomsen, W., Hauser, E., Whelan, K., Grottick, A.J., 2008. A new family of H3 receptor antagonists based on the natural product Conessine. Bioorg. Med. Chem. Lett. 18, 1490–1494. https://doi.org/10.1016/j.bmcl.2007.12.059.

Seeliger, D., De Groot, B.L., 2010. Ligand docking and binding site analysis with PyMOL and Autodock/Vina. J. Comput. Aided Mol. Des. 24, 417–422. https://doi.org/10.1007/s10822-010-9352-6.

Sheikh, Y., Manral, M.S., Kathait, V., Kumar, R., Sahu, R.A.M.K., 2015. Computation of In Vivo Antidiabetic Activity of *Holarrhena antidysenterica* Seeds Extracts in Streptozotocin-Induced Diabetic Rats. Vol. 14. pp. 22–27.

Shen, M.Y., Sali, A., 2006. DOPE score-statistical potential for assessment and prediction of protein structures. Protein Sci. 15, 2507–2524. https://doi.org/10.1110/ps.062416606.

Singh, R., Chandra, S., Dhusia, K., Sharma, G., 2016. Capacitating surveillance and situational awareness with measure of visual engagement using eyetracker, in: 2016 International Conference on Computing, Communication and Automation (ICCCA). IEEE Xplore 1161–1165. https://doi.org/10.1109/CCAA.2016.7813892.

Smith, R., Coast, J., 2013. The true cost of antimicrobial resistance. BMJ 346https://doi.org/10.1136/bmj.f1493. f1493–f1493.

Soheilifard, R., Makarov, D.E., Rodin, G.J., 2008. Critical evaluation of simple network models of protein dynamics and their comparison with crystallographic B-factors. Phys. Biol. 5, 026008. https://doi.org/10.1088/1478-3975/5/2/026008.

Su, L.-H., Ou, J.T., Leu, H.-S., Chiang, P.-C., Chiu, Y.-P., Chia, J.-H., Kuo, A.-J., Chiu, C.-H., Chu, C., Wu, T.-L., Sun, C.-F., Riley, T.V., Chang, B.J., 2003. Extended epidemic of nosocomial urinary tract infections caused by Serratia marcescens. J. Clin. Microbiol. 41, 4726–4732. https://doi.org/10.1128/JCM.41.10.4726-4732.2003.

Su, G., Morris, J.H., Demchak, B., Bader, G.D., 2014. Biological Network Exploration with Cytoscape 3, in: Current Protocols in Bioinformatics. John Wiley & Sons, Inc., Hoboken, NJ, USA. https://doi.org/10.1002/0471250953.bi0813s47. (pp. 8.13.1–8.13.24).

Szklarczyk, D., Franceschini, A., Wyder, S., Forslund, K., Heller, D., Huerta-Cepas, J., Simonovic, M., Roth, A., Santos, A., Tsafou, K.P., Kuhn, M., Bork, P., Jensen, L.J., Von Mering, C., 2015. STRING v10: protein-protein interaction networks, integrated over the tree of life. Nucleic Acids Res. 43, D447–D452. https://doi.org/10.1093/nar/gku1003.

Tadaka, S., Kinoshita, K., 2016. NCMine: core-peripheral based functional module detection using near-clique mining. Bioinformatics 32, 3454–3460. https://doi.org/10.1093/bioinformatics/btw488.

Thompson, R.L., Cabezudo, I., Wenzel, R.P., 1982. Epidemiology of nosocomial infections caused by methicillin-resistant Staphylococcus aureus. Ann. Intern. Med. 97, 309–317. https://doi.org/10.7326/0003-4819-97-3-309.

Trott, O., Olson, A.J., 2010. AutoDock Vina: improving the speed and accuracy of docking with a new scoring function, efficient optimization, and multithreading. J. Comput. Chem. 31, 455–461. https://doi.org/10.1002/jcc.21334.

Trubiano, J.A., Padiglione, A.A., 2015. Nosocomial infections in the intensive care unit. Anaesth. Intensive Care Med. https://doi.org/10.1016/j.mpaic.2015.09.010.

Vitali, J., Carroll, D., Chaudhry, R.G., Hackert, M.L., 1999. Three-dimensional structure of the Gly121Tyr dimeric form of ornithine decarboxylase from Lactobacillus 30a. Acta Crystallogr. Sect. D Biol. Crystallogr. 55, 1978–1985. https://doi.org/10.1107/S0907444999010756.

Vrijens, F., Gordts, F., De Laet, B., 2009. Nosocomiale infecties in België, Deel II: impact op Mortaliteit en Kosten. Health Serv. Res. 1–108.

Wallace, H.M., Fraser, A.V., 2004. Inhibitors of polyamine metabolism: review article. Amino Acids 26, 353–365. https://doi.org/10.1007/s00726-004-0092-6.

Webb, B., Sali, A., 2014. Comparative protein structure modeling using MODELLER. Curr. Protoc. Bioinformatics 2014https://doi.org/10.1002/0471250953.bi0506s47. 5.6. 1–5.6.32.

Wiederstein, M., Sippl, M.J., 2007. ProSA-web: interactive web service for the recognition of errors in three-dimensional structures of proteins. Nucleic Acids Res. 35. https://doi.org/10.1093/nar/gkm290.

Yu, V.L., 1979. Serratia marcescens — historical perspective and clinical review. N. Engl. J. Med. 300, 887–893. 10.1056.

Zhang, Z., Li, Y., Lin, B., Schroeder, M., Huang, B., 2011. Identification of cavities on protein surface using multiple computational approaches for drug binding site prediction. Bioinformatics 27, 2083–2088. https://doi.org/10.1093/bioinformatics/btr331.

Zhang, Q.C., Petrey, D., Deng, L., Qiang, L., Shi, Y., Thu, C.A., Bisikirska, B., Lefebvre, C., Accili, D., Hunter, T., Maniatis, T., Califano, A., Honig, B., 2012. Structure-based prediction of protein–protein interactions on a genome-wide scale. Nature 490, 556–560. https://doi.org/10.1038/nature11503.

Zingg, W., Holmes, A., Dettenkofer, M., Goetting, T., Secci, F., Clack, L., Allegranzi, B., Magiorakos, A.-P., Pittet, D., systematic review and evidence-based guidance on organization of hospital infection control programmes (SIGHT) study group, 2015. Hospital organisation, management, and structure for prevention of health-care-associated infection: a systematic review and expert consensus. Lancet Infect. Dis. 15, 212–224. https://doi.org/10.1016/S1473-3099(14)70854-0.